STATE RESEARCH CENTER OF RUSSIA

INSTITUTE FOR HIGH ENERGY PHYSICS

IHEP 2002-23

V.V. Zmushko

SEARCH FOR $H \to \gamma\gamma$ IN THE REACTION $pp \to H + jet + X$ AT $\sqrt{s} = 14$ TeV

Submitted to *Yad. Fiz.*

Protvino 2002

UDK 539.12.13.348 M–24

Abstract

Zmushko V.V. Search for $H \to \gamma\gamma$ in the Reaction $pp \to H + jet + X$ at $\sqrt{s} = 14$ TeV: IHEP Preprint 2002-23. – Protvino, 2002. – p. 13, figs. 8, tables 5, refs.: 17.

The possibility of the LHC for finding the Standard Model Higgs boson in the $H \to \gamma\gamma$ decay mode is discussed for the case of the Higgs production in association with one jet. The detailed simulation of the signal and the backgrounds was carried out. For signal the different approaches are compared which led to a similar results after the choice of the proper cuts and normalization. The $pp \to \gamma\gamma + jet + X$ background was generated with the exact matrix-elements. The parton-shower, hadronization and detector simulation influence on results was studied. The ATLAS detector parameters were used for the detector responce simulation. It was found the result dependence with respect to the choice of the parton-showering scale Q for the background. In any case, for $m_H = 115 \div 140$ GeV the signal significance was evaluated about or above 5 for an integrated luminosity of 30 fb^{-1}.

Аннотация

Змушко В.В. Поиск $H \to \gamma\gamma$ в реакции $pp \to H + jet + X$ при $\sqrt{s} = 14$ ТэВ: Препринт ИФВЭ 2002-23. – Протвино, 2002. – 13 с., 8 рис., 5 табл., библиогр.: 17.

Изучена возможность обнаружения на коллайдере LHC хиггсовского бозона, предсказываемого Стандартной моделью, в моде распада $H \to \gamma\gamma$ при его образовании в сопровождении струи. Проведен детальный анализ сигнала и фона. Рассмотрены разные подходы моделирования образования хиггса. Показано, что они дают одинаковые результаты при правильном выборе обрезаний и нормировки. Фоновый процесс $pp \to \gamma\gamma + jet + X$ моделировался с использованием точных матричных элементов. Изучено влияние на полученные результаты как учета при моделировании сигнала и фона образования партонных ливней и адронизации партонов, так и параметров детектора. В качестве детектора рассматривалась установка ATLAS. Обнаружена зависимость результатов от выбора масштаба Q, используемого при описании партонных ливней в фоновых процессах. В любом случае для интегральной светимости 30 фб$^{-1}$ и $m_H = 115 \div 140$ ГэВ значимость сигнала оценивается величиной около или выше 5.

Introduction

The Higgs boson search at LEP established a 95% confidence-level lower limit for the Standard Model Higgs boson of 111.5 GeV [1]. The 3σ excess of events above background which are compatible with the Higgs boson of mass $m_H = 115$ GeV is also observed [1]-[4]. In this mass region the $H \to \gamma\gamma$ channel is considered as the main channel for the Higgs search at LHC. However, for this channel the signal-to-background (S/B) ratio is very low. For ATLAS detector the extraction of the Higgs signal requires one year of running at high luminosity [5]. The production of the Higgs in association with large p_T jet can be used to improve the $H \to \gamma\gamma$ signal significance and S/B ratio. The specific jet distributions in the $\gamma\gamma$ + jet final state are different for signal and background processes. Promising results were obtained in the parton-level study [6]. It was shown that, selecting of the jet with $p_T > 30$ GeV and using the cut on the partonic subprocess energy $\sqrt{\hat{s}}$, the S/B ratio could be significantly improved and the discovery level $S/\sqrt{B} = 5$ could be achieved for $m_H = 110 \div 140$ GeV for the integrated luminosity of 30 fb^{-1}, which correspondes to three years of running at low luminosity. The goal of this study is to reproduce above-described results on particle-level with detector simulation. Some estimates were done in [7] where PYTHIA 5.7 [8] was used to generate the signal and background events. Here the signal events were generated by PYTHIA 6.2 [9]. For the background calculation the events from the $2 \to 3$ subprocesses were generated with exact matrix-elements by CompHEP package [10] and then they were used as an input to PYTHIA 6.2. The detector response was simulated with ATLFAST package [11].

1. Selection criteria and cuts

The event selection criteria are similar to the set 2 in the analysis performed in [6]:

- 2 isolated photons with $p_T^\gamma > 40$ GeV and $|\eta_\gamma| < 2.5$,
- at least one jet with $p_T^{jet} > 30$ GeV and $|\eta_{jet}| < 4.5$.

The events with one or more photons in region of the electro-magnetic barrel/endcap transition, $1.42 < |\eta| < 1.57$, were rejected.

The γ-jet separation $\Delta R = \sqrt{\Delta\phi^2 + \Delta\eta^2} = 0.4$ was determined by the photons isolation criteria in ATLFAST.

It has been found in [6] that the background events from the $gq \to \gamma + \gamma + q$ and $q\bar{q} \to \gamma + \gamma + g$ subprocesses have a smaller $\sqrt{\hat{s}}$ than the signal events from $gg \to gH$, $qg \to qH$ and $q\bar{q} \to gH$ and the cut on $\sqrt{\hat{s}}$ is very useful. On parton-level study one has $\sqrt{\hat{s}} = M_{\gamma\gamma jet}$. In this study the cut on $M_{\gamma\gamma jet}$ was imposed, where the jet with the largest p_T was selected for the multi-jet final states.

2. Signal and background generation

2.1. Signal

The $2 \to 2$ QCD subprocesses $gg \to gH$, $qg \to qH$ and $q\bar{q} \to gH$ are commonly considered as source of the $H + jet$ events with large p_T. On the other hand the parton emission from the initial partons in the fusion subprocesses $gg \to H$ and $q\bar{q} \to H$ can also produce jets with $p_T < m_H$. In PYTHIA 6.2 the parton emission in the $gg \to H$ fusion process is corrected by the ratio of the matrix-elements square of the $2 \to 2$ processes to the probability of the parton emission, and the shower-generator limit $Q_{max} = m_H$ is replaced by $Q_{max} = \sqrt{s}$ to extend the p_T range up to $\sqrt{s}/2$. Note that the other partons from the backwards shower evolution have smaller p_T due to p_T-ordering. The $gg \to H$ fusion process with the matrix-element corrections (process ISUB = 103 in PYTHIA 6.2) can be used for the description $H + jet$ production for all p_T values of jet. This approach applied to the $W + jet$ production at the Tevatron [12] gives a good discription of the experimental data from the D0 collaboration [13]. In this study both approaches, i.e. $2 \to 2$ and $gg \to H$ with the matrix-element corrections, are considered and compared. The contribution from the process $q\bar{q} \to gH$ and $q\bar{q} \to H$ is small and can be neglected.

The $H + jet$ events can be produced also in the WW or ZZ fusion subprocesses $qq \to qqH$ and in the Higgs production associated with W, Z where the vector boson decays into a quark-antiquark pair.

The events were generated by PYTHIA version 6.202 with the default CTEQ 5L parton-distribution set. The same values for $Br(H \to \gamma\gamma)$ were used as it was done for the $H \to \gamma\gamma$ channel study in [5].

As usual the cut is imposed on $\hat{p}_T$ to exclude singularity in the $2 \to 2$ processes when the parton showering is on. Here $\hat{p}_T$ is a parton transverse momentum in the rest frame of the hard interaction. The two cases $\hat{p}_T > 10$ GeV and 20 GeV are considered.

In PYTHIA 6.2 the $gg \to H$ process with the matrix-element corrections is normalized in order to have the same value for the total cross-section as for the $gg \to H$ process without corrections. In this study the factor 1.5 is included in order to have the cross-section value for large p_T^H the same as for $2 \to 2$ processes, which describe the LO large p_T Higgs production. In fact, though the $2 \to 2$ processes contribute to the NLO total cross-section, the NLO corrections mainly come from soft- and virtual-gluon effects and factorize into K-factor. Note, that the NLO K-factor for $gg \to H$ is about 1.7 for $m_H = 100 \div 150$ GeV [14]. Thus, we have a correct LO behaviour for large p_T and the NLO total cross-section. The NLO corrections are also calculated for large p_T Higgs production and K-factor is about 1.6 [15]. This K-factor is not included here.

In Fig. 1 the p_T^H and p_T^{jet} distributions for the $gg \to H$ fusion process with the matrix-element corrections are compared with the distributions for the $2 \to 2$ processes with and without parton showering. There is good agreement between the $d\sigma/dp_T^H$ cross-sections calculated within the $gg \to H$ with the matrix-element corrections and $2 \to 2$ approaches for $p_T^H > m_H$. The $d\sigma/dp_T^{jet}$

cross-sections for the $gg \to H$ with the matrix-element corrections and the $2 \to 2$ processes without showering have about the same values for p_T^{jet} >30 GeV. The $d\sigma/dp_T^{jet}$ for the $2 \to 2$ processes with showering has a slightly different p_T -dependence.

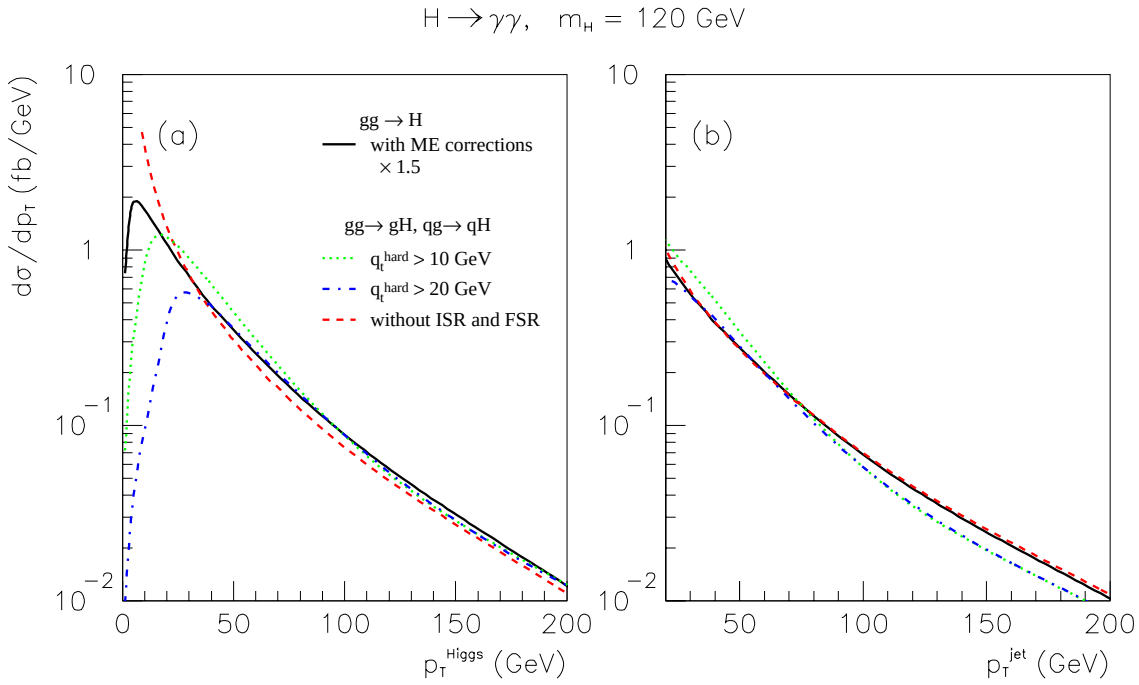

Fig. 1. The p_T^H (a) and p_T^{jet} (b) distributions for Higgs production processes in the case $m_H = 120$ GeV.

The $2 \to 2$ processes approach with parton-showering and $\hat{p}_T > 10$ GeV overestimates the cross-section for the low p_T range. In this case the part of the cross-section is saturated by the soft $2 \to 2$ interaction. It can be seen from Fig. 2 where we present the $\hat{p}_T$ distribution for events with $p_T^{jet} > 30$ GeV. The cut $\hat{p}_T > 20$ GeV provides the rejection of the contribution from the soft interaction.

The $M_{\gamma\gamma jet}$ distributions are shown in Fig. 3(a, b). There is a good agreement between the $gg \to H$ approach and the $2 \to 2$ approach with the cut $\hat{p}_T > 20$ GeV for $M_{\gamma\gamma jet}$ >250 GeV. If $\hat{p}_T > 10$ GeV, the agreement is better for low values of $M_{\gamma\gamma jet}$. We can compare the $M_{\gamma\gamma jet}$ distribution with the $\sqrt{\hat{s}}$ distribution for the $gg \to Hg$, $gq \to Hq$ events. The distributions are very similar for $M_{\gamma\gamma jet} > 250$ GeV. Fig. 3(c, d) shows the same distributions after the cut $M_{\gamma\gamma jet} > 300$ GeV. Some contribution from the low $\sqrt{\hat{s}}$ region is noticeable here. In particular, about 20% of the contribution is coming from the $\sqrt{\hat{s}} < 240$ GeV region in the case of the $\hat{p}_T > 10$ GeV cut. The events from the $\sqrt{\hat{s}} < 240$ GeV region have the low values of $\hat{p}_T$ and $p_T^{jet} < m_H$ (see Fig. 2(c, d)). This implies that the selected jet is not from the final state of the $2 \to 2$ interaction but is emited from the initial parton. The corresponded Feynman diagram contributes to NLO corrections. There is no ambiguity of the jet selection for the $gg \to H$ approach with the matrix-element corrections because p_T-ordering of the partons.

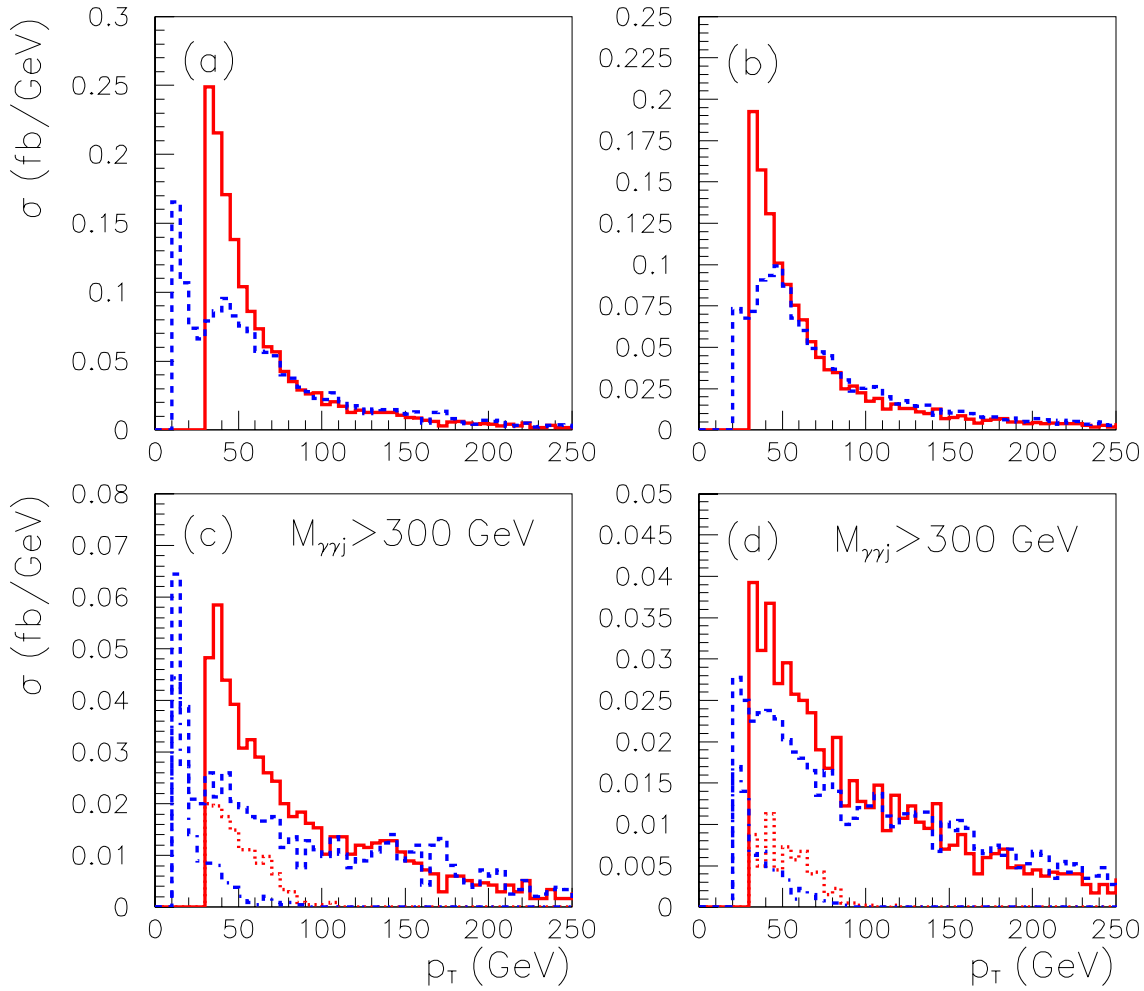

Fig. 2. The p_T^{jet} distribution for the $gg \to Hg$, $gq \to Hq$ events after applying the photons and jet selection criteria without (a, b) and with the $M_{\gamma\gamma jet} > 300$ GeV cut (c, d) in the case $m_H = 120$ GeV. The events were generated with the cut $\hat{p}_T > 10$ GeV (a, c) , $\hat{p}_T > 20$ GeV (b, d). The dashed line corresponds to the $\hat{p}_T$ distribution for the same events. The p_T^{jet} (dotted line) and $\hat{p}_T$ (dot-dashed line) distributions for the events with $\sqrt{\hat{s}} < 240$ GeV are also shown in the case of the $M_{\gamma\gamma jet} > 300$ GeV cut.

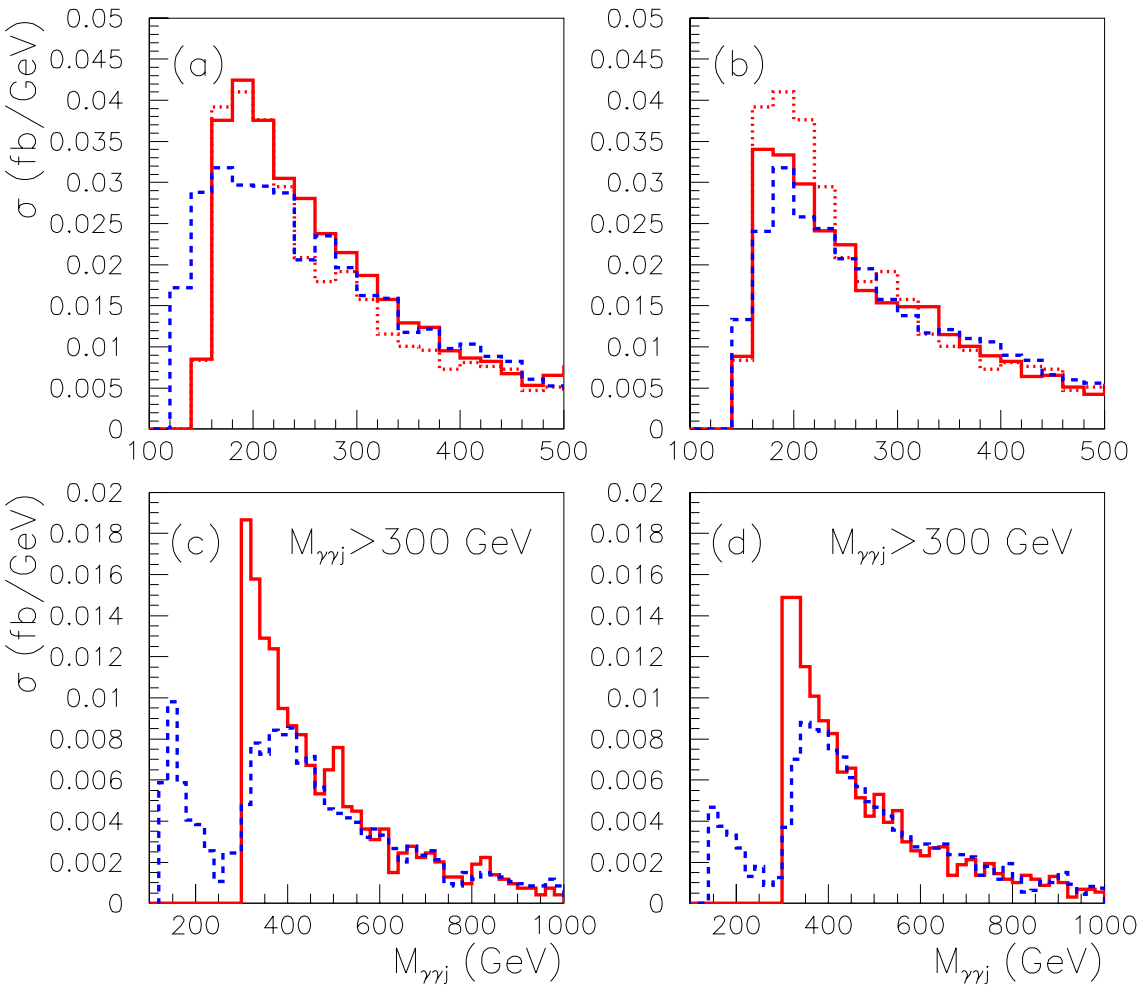

Fig. 3. The $M_{\gamma\gamma jet}$ distribution for the $gg \to Hg$, $gq \to Hq$ events after applying the photons and jet selection criteria without (a, b) and with the $M_{\gamma\gamma jet} > 300$ GeV cut (c, d) in the case $m_H = 120$ GeV. The events were generated with the cut $\hat{p}_T > 10$ GeV (a, c) , $\hat{p}_T > 20$ GeV (b, d). The dashed line corresponds to the parton c.m. energy $\sqrt{\hat{s}}$ distribution for the same events. The dotted line corresponds to the $M_{\gamma\gamma jet}$ distribution for the $gg \to H$ events.

2.2. Background

The background consists of the the irreducible background from the reaction $pp \to \gamma\gamma + jet + X$ and the reducible one from the reactions $pp \to \gamma + jet + jet + X$ and $pp \to jet + jet + jet + X$ where one or two jets are misidentified as photons. The reducible background is estimated with PYTHIA 5.7 simulation [7] and consists of about 10% from the irreducible one. In this study the reducible background is not considered.

At LO level the irreducible background receives contributions from the $gq \to \gamma + \gamma + q$ and $q\bar{q} \to \gamma + \gamma + g$ subprocesses.

For the $\gamma\gamma$ channel the contribution from the NLO one-loop subprocess $gg \to \gamma + \gamma$ is same as the contribution from the LO subprocess $q\bar{q} \to \gamma + \gamma$ because the parton-luminosity is rather low for the $q\bar{q}$ initial state. For the $\gamma\gamma$+jet channel the contribution from the NLO one-loop

subprocess $gg \to \gamma + \gamma + g$ is less than 20% of the LO contributions [16] and can be neglected for this study.

The CompHEP 33.23 package [10] was used for calculation of the matrix-elements for the $gq \to \gamma + \gamma + q$ and $q\bar{q} \to \gamma + \gamma + g$ subprocesses and then for generation of $pp \to \gamma + \gamma + q(g)$ events with weights.

For this study CompHEP was linked with PDFLIB [17]. The CTEQ5 L parton-distribution set and the corresponded α_S was used for the background calculation the same as for the signal generation. The Q^2 definition was changed to correspond to the PYTHIA Q^2 definition for the $gg \to (H \to \gamma\gamma) + g$ and $gq \to (H \to \gamma\gamma) + q$ signal subprocesses $Q^2 = 0.5M^2_{\gamma\gamma} + (p_T^{q(g)})^2$. The electroweak coupling value was 1/137.036 since the photons are on-shell (the default CompHEP choice is $\alpha(M_Z) = 1/128.9$).

The following cuts were imposed on the parton kinematical variables:

- $p_T^{\gamma} > 30$ GeV (25 GeV , for m_H= 110 GeV),
- $p_T^{jet} > 20$ GeV,
- $|\eta_{\gamma}| < 3$,
- $|\eta_{jet}| < 5$,
- $\Delta R_{\gamma q(g)} > 0.3$,
- $\Delta R_{\gamma\gamma} > 0.3$.

The parton cuts are looser than the cuts for the reconstructed photons and jets because the kinematical variables of photons and jets differ from the kinematical variables of their parent partons after the parton-showering, the hadronization and the detector simulation. The parton cuts were chosen in such a way as to minimize their influence on the kinematical variables distributions for the reconstructed jets and photons and to exclude the singular regions of the parton kinematical variables.

The events with weights from CompHEP were converted to an unweighted event samples and saved on the disk. The parton-showering and the hadronization was generated by PYTHIA version 6.202 where the unweighted parton-level events were considered as events from the external process.

To generate events by PYTHIA with external process one needs to set the Q scale for parton-showering. The common choice is the scale, as used in the calculation of parton distribution, i.e. $Q^2 = 0.5M^2_{\gamma\gamma} + (p_T^{q(g)})^2$. In this case p_T of the jet emited from the initial parton can be larger than p_T of the jet from the hard subprocess. The more preferable choice from the point of view of the physical pattern of the process and the LO approximation is $Q^2 = (p_T^{q(g)})^2$. In this case the selected jet with the largest p_T always results from the hard subprocess and there is no double counting of Feynman diagrams. The three cases were considered here to study the parton-shower influence on the results: 1) $Q^2 = (p_T^{q(g)})^2$, 2) $Q^2 = 0.5M^2_{\gamma\gamma} + (p_T^{q(g)})^2$ and 3) $Q^2 = M^2_{\gamma\gamma} + 2(p_T^{q(g)})^2$.

The background cross-section was averaged on $M_{\gamma\gamma}$ within the $m_H \pm 5$ GeV interval.

Fig. 4÷5 show the p_T^{jet} and $M_{\gamma\gamma jet}$ distributions for the reconstructed photons and jet in comparison with the corresponded distributions for photons and quark (gluon) in final state of the underlaying parton subprocess after applying the event selection criteria and before and after the $M_{\gamma\gamma jet} > 300$ GeV cut in the case m_H= 120 GeV. We can see that the p_T^{jet} and $M_{\gamma\gamma jet}$ distributions are similar to the $p_T^{q(g)}$ and $\sqrt{\hat{s}}$ distributions if $Q^2 = (p_T^{q(g)})^2$ for parton-showering. For $Q^2 = 0.5M^2_{\gamma\gamma} + (p_T^{q(g)})^2$ the parton interaction with low $\sqrt{\hat{s}}$ contributes to the events with

$M_{\gamma\gamma jet} > 300$ GeV (see Fig. 5(d)). It could be possible if the selected jet which has the largest p_T is emited from the initial parton but not from the hard interaction as it is described above for the signal. The contribution from the low $\sqrt{\hat{s}}$ region can be considered as some correction to the LO approximation. This contribution is about 30% for $\sqrt{\hat{s}} < 240$ GeV and increases with value of the $M_{\gamma\gamma jet}$ cut, e.g. it is about 38% for $M_{\gamma\gamma jet} > 400$ GeV. The events which have $\sqrt{\hat{s}} < 240$ GeV saturate the low p_T region (see Fig. 4(d)).

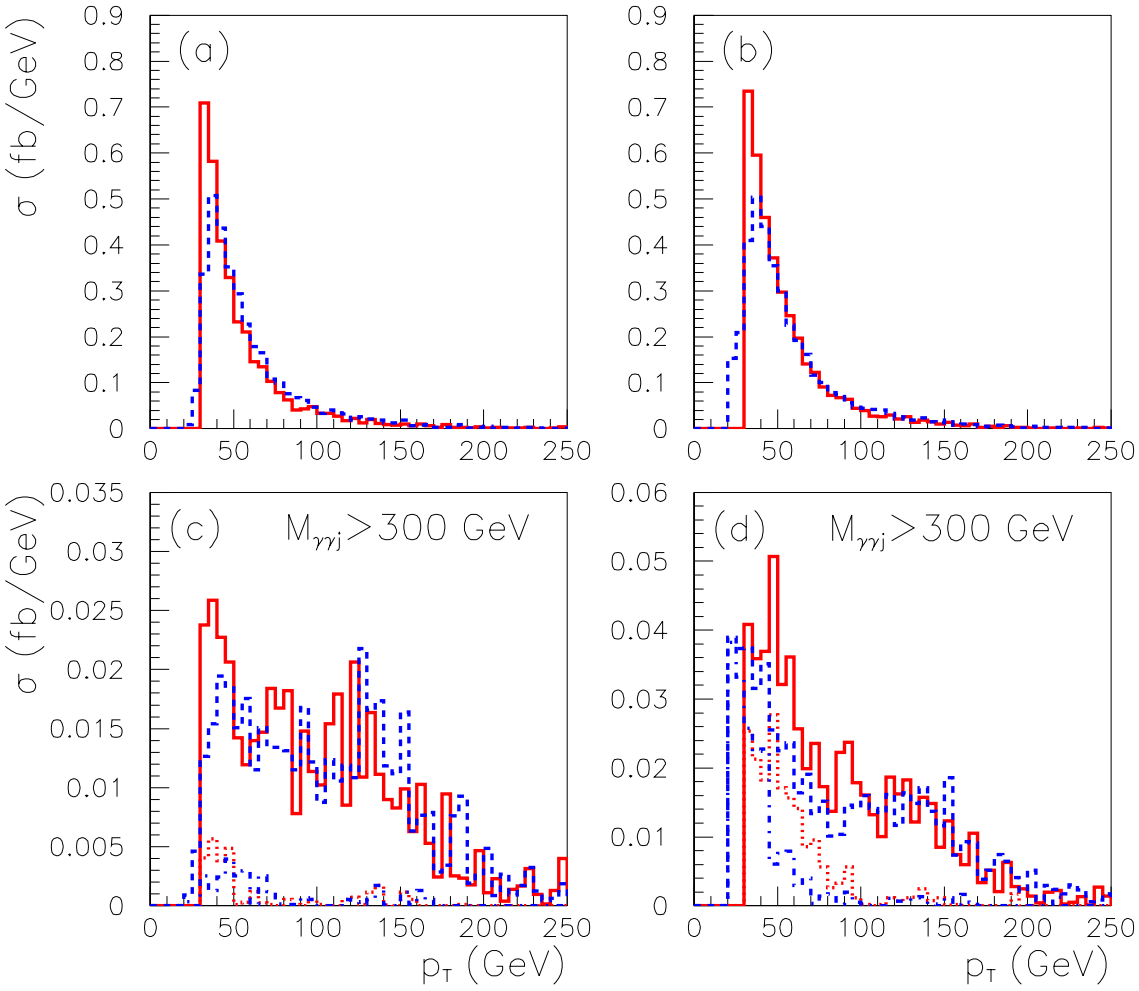

Fig. 4. The p_T^{jet} distribution for the background after applying the photons and jet selection criteria without (a, b) and with the $M_{\gamma\gamma jet} > 300$ GeV cut (c, d) in the case $m_H = 120$ GeV. The parton showering was simulated with $Q^2 = (p_T^{q(g)})^2$ (a, c) and $Q^2 = 0.5M_{\gamma\gamma}^2 + (p_T^{q(g)})^2$ (b, d). The dashed line corresponds to the $p_T^{q(g)}$ before parton-showering distribution for the same events. The p_T^{jet} (dotted line) and $p_T^{q(g)}$ (dot-dashed line) distributions for the events with $\sqrt{\hat{s}} < 240$ GeV are also shown in the case of the $M_{\gamma\gamma jet} > 300$ GeV cut.

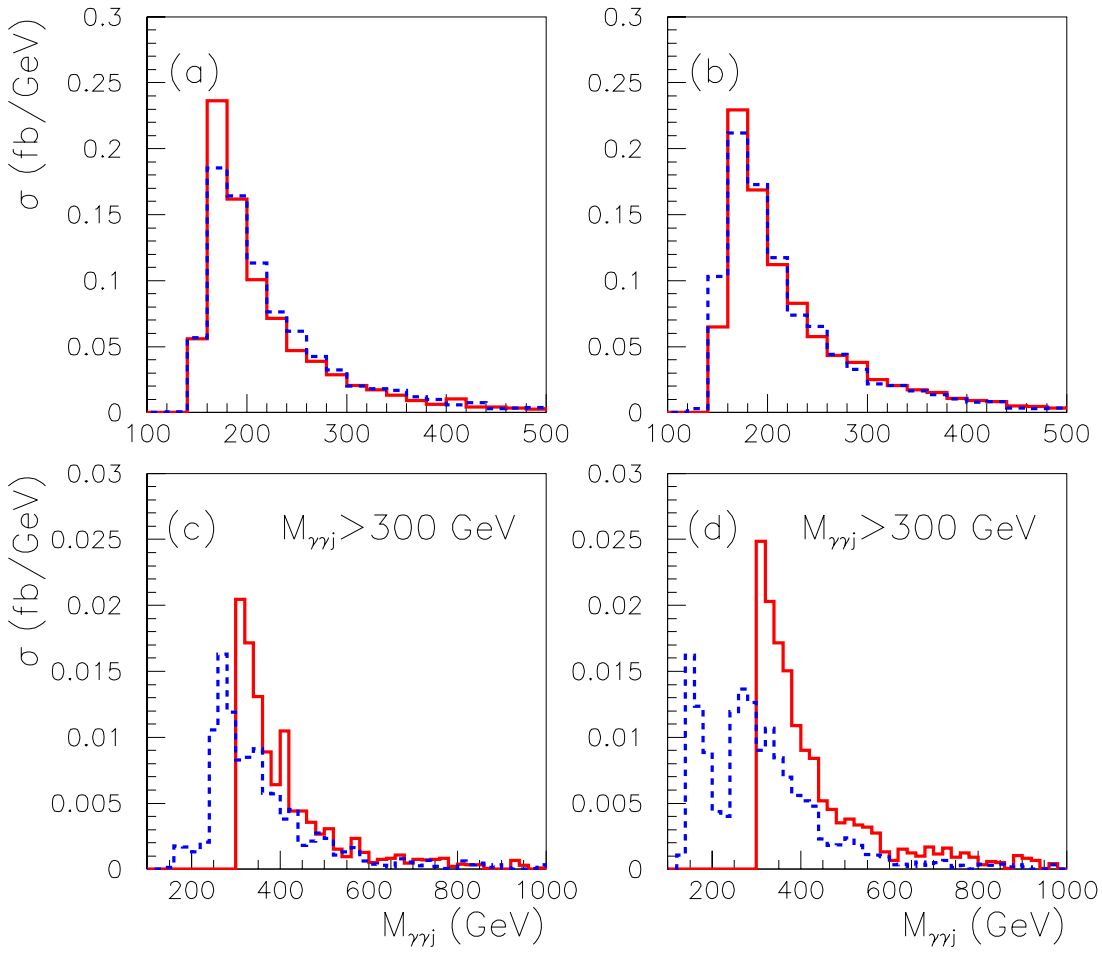

Fig. 5. The $M_{\gamma\gamma jet}$ distribution for the background after applying the photons and jet selection criteria without (a, b) and with the $M_{\gamma\gamma jet} > 300$ GeV cut (c, d) in the case $m_H = 120$ GeV. The parton showering was simulated with $Q^2 = (p_T^{q(g)})^2$ (a, c) and $Q^2 = 0.5M_{\gamma\gamma}^2 + (p_T^{q(g)})^2$ (b, d). The dashed line corresponds to the parton c.m. energy $\sqrt{\hat{s}}$ distribution for the same events.

3. Results

The production cross-sections for the Higgs boson with $m_H = 120$ GeV generated with QCD processes after applying the photons and jet selection criteria and after the $M_{\gamma\gamma jet} > 300$ GeV cut are presented in Table 1 for the following approaches for Higgs production:

1. $gg \to H$ fusion process with ME corrections and factor 1.5;
2. $gg \to Hg, gq \to Hq$ subprocesses with $\hat{p}_T > 20$ GeV;
3. $gg \to Hg, gq \to Hq$ subprocesses with $\hat{p}_T > 20$ GeV without ISR and FSR;
4. $gg \to Hg, gq \to Hq$ subprocesses with $\hat{p}_T > 10$ GeV.

The cross-sections for the parton-level calculation are also shown in this Table. The difference from the corresponding cross-sections in the parton-level study [6] is mainly due to the ATLAS barrel/endcap crack. About 10% of events is lost because the efficiencies of the reconstruction of isolated photons and jets are not 100% and the momentum rescaling. As expected, the $2 \to 2$ subprocesses with the $\hat{p}_T > 10$ GeV cut, which is too low, overestimate the cross-sections. The parton-showering has small influence on the cross-sections for Higgs production in the case $2 \to 2$ interaction with the proper choice of $\hat{p}_T$ cut. The results are very similar in the case 1 and 2. In what follows the approach 1 is used as more consistent.

Table 1. The production cross-section (in fb) of Higgs boson with $m_H = 120$ GeV before and after cuts for cases: 1) $gg \to H$ with ME corrections and factor 1.5; 2) $gg \to Hg, gq \to Hq$, $\hat{p}_T > 20$ GeV; 3) $gg \to Hg, gq \to Hq$, $\hat{p}_T > 20$ GeV without ISR and FSR; 4) $gg \to Hg, gq \to Hq$, $\hat{p}_T > 10$ GeV. The cross-sections for the parton-level calculation are also shown.

	Total	Photons and jet selection	$M_{\gamma\gamma jet}$ >300 GeV
Parton-level	31.27	8.02	3.23
1	60.69	7.12	2.85
2	31.27	6.65	2.95
3	31.27	6.95	2.97
4	53.35	7.99	3.39

The cross-sections for the background events in the case $m_H = 120$ GeV after applying the photons and jet selection criteria and after the $M_{\gamma\gamma jet} > 300$ GeV cut are presented in Table 2 for the parton-level calculation, the calculation with and without the parton-showering with the hadronization and the detector simulation.

Table 2. The cross-section (in fb) for the background events in the case $m_H = 120$ GeV after applying the photons and jet selection criteria and after the $M_{\gamma\gamma jet} > 300$ GeV cut.

	Photons and jet selection	$M_{\gamma\gamma jet}$ >300 GeV
Parton-level	21.38	2.57
No parton showering	18.39	2.55
FSR, $Q^2 = (p_T^{q(g)})^2$	16.64	2.22
ISR + FSR, $Q^2 = (p_T^{q(g)})^2$	17.04	2.23
Same, $Q^2 = 0.5M_{\gamma\gamma}^2 + (p_T^{q(g)})^2$	19.05	3.11
Same, $Q^2 = M_{\gamma\gamma}^2 + 2(p_T^{q(g)})^2$	20.39	3.52

The inclusion of the detector simulation and FSR reduces the cross-section. The ISR increases the cross-section. The increase is very small for the $Q^2 = (p_T^{q(g)})^2$ choice for the parton-showering. The default PYTHIA choice $Q^2 = 0.5M_{\gamma\gamma}^2 + (p_T^{q(g)})^2$ is used in what follows to be conservative.

Table 3 shows the comparison of the cross-sections for the signal and background events and the contribution of the different channels. The cross-sections for the QCD and EW Higgs production are about the same after the $M_{\gamma\gamma jet} > 300$ GeV cut. In [6] only one jet with $p_T^{jet} > 30$ GeV and $|\eta_{jet}| < 4.5$ is required. This requirement suppresses the contribution from the EW Higgs production.

The background processes contribute at a smaller $M_{\gamma\gamma jet}$ in comparison with the signal processes (see Fig. 6). The $M_{\gamma\gamma jet} > 300$ GeV cut reduces the background by a factor of 6.1 while the signal is reduced only by a factor of 2.2.

Table 3. The cross-section (in fb) for the signal and background events for $m_H = 120$ GeV before and after applying the photons and jet selection criteria and the $M_{\gamma\gamma jet} > 300$ GeV cut.

Process	Total	Photons and jet selection	$M_{\gamma\gamma jet}$ >300 GeV
$gg \to H$	60.69	7.12	2.85
$qq \to qqH$	9.26	3.13	2.05
$WH,\ ZH$	4.28	0.98	0.23
Signal	74.23	11.24	5.13
$gq \to \gamma\gamma q$		16.84	2.57
$q\bar{q} \to \gamma\gamma g$		2.21	0.54
bgd./1 ГэВ		19.05	3.11

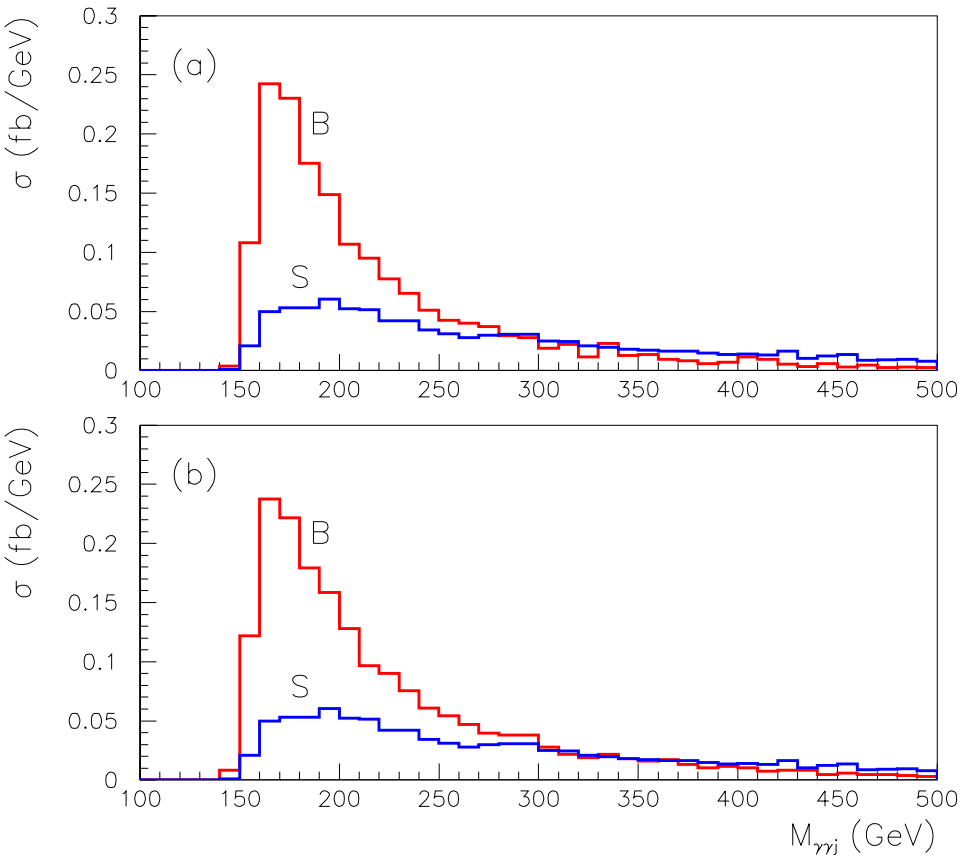

Fig. 6. The $M_{\gamma\gamma jet}$ distribution for the signal (S) and background (B) after applying the photons and jet selection criteria in the case $m_H = 120$ GeV. The parton showering for the background was simulated with (a) $Q^2 = (p_T^{q(g)})^2$ and (b) $Q^2 = 0.5M_{\gamma\gamma}^2 + (p_T^{q(g)})^2$. The background normalization corresponds to the $M_{\gamma\gamma}$ bin of 1 GeV.

For the evaluation of the number of the signal and background events the $M_{\gamma\gamma}$ interval of $\pm 1.4\sigma = 3.64$ GeV was used with $\sigma = 1.3$ GeV [5]. This interval contains 80% of the signal events. The photon identification efficiency of 80% per photon is assumed.

The numbers of the signal and background events, the S/B ratios and the signal significances $S/\sqrt{B}$ for an integrated luminosity of 30 fb^{-1} are shown in Table 4 after applying the photons and jet selection criteria and in Table 5 after $M_{\gamma\gamma jet}$ >300 GeV cut.

Table 4. The number of the signal and background events, the S/B ratio and the significances after applying the photons and jet selection criteria for an integrated luminosity of 30 fb^{-1}.

m_H (GeV)	110	120	130	140
S	138	173	178	157
B	1246	1332	1402	1301
S/B	0.11	0.13	0.13	0.12
$S/\sqrt{B}$	3.91	4.73	4.76	4.36

Table 5. The number of the signal and background events, the S/B ratio and the significances after applying the photons and jet selection criteria and after the $M_{\gamma\gamma jet} > 300$ GeV cut for an integrated luminosity of 30 fb^{-1}.

m_H (GeV)	110	120	130	140
S	63	79	90	85
B	203	217	246	260
S/B	0.31	0.36	0.36	0.33
$S/\sqrt{B}$	4.44	5.34	5.71	5.29

The dependence of the S/B ratio and the significance on the $M_{\gamma\gamma jet}$ cut is shown in Fig. 7. The S/B ratio is significantly improved with increasing of the $M_{\gamma\gamma jet}$ cut value. $S/\sqrt{B}$ varies slowly and has a maximum at the cut value about 300 GeV.

Fig. 8 illustrates the m_H dependence of the S/B ratio and the signal significance. The results are presented for the different choices of Q^2 for the parton-showering in the background calculations. The significance is above 5 for m_H= 110÷140 GeV in case $Q^2 = p_T^{q(g)}$ which corresponds the LO approximation. In other cases, where there is a contribution corresponded the NLO corrections, the significance and S/B ration has some low values. Note that the NLO K-factor for the large p_T Higgs production is not included here.

4. Conclusions

The detailed simulation of the signal and the background for $H(\to \gamma\gamma) + jet$ channel have been carried out for the LHC. The promising results of the parton-level study [6] have been confirmed.

The different approaches for signal generation led to a similar results after the choice of the proper cuts and normalization. The background cross-section slightly differs from the parton-level estimate if the parton-showering generation corresponds the LO approximation. The more conservative approach yields a factor of $1.2 \div 1.4$.

In any case, for m_H= $115 \div 140$ GeV the signal significance was evaluated about or above 5 for an integrated luminosity of 30 fb^{-1}. The S/B ratio could reach the values of $0.3 \div 0.5$.

Acknowledgements

I would like to thank E.A. Kozlovsky and E. Richter-Was for many valuable comments.

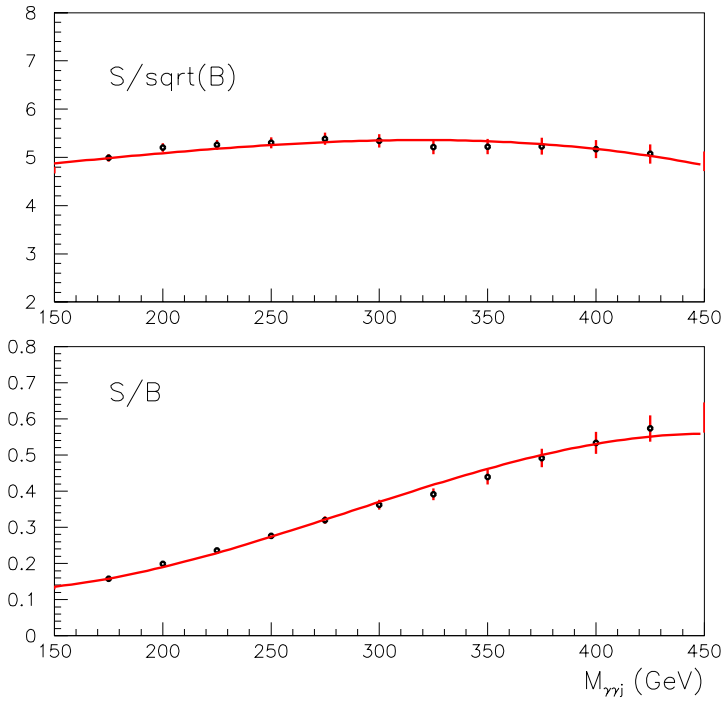

Fig. 7. The significance and the S/B ratio vs.$M_{\gamma\gamma jet}$ for an integrated luminosity of 30 fb^{-1} in the case $m_H = 120$ GeV.

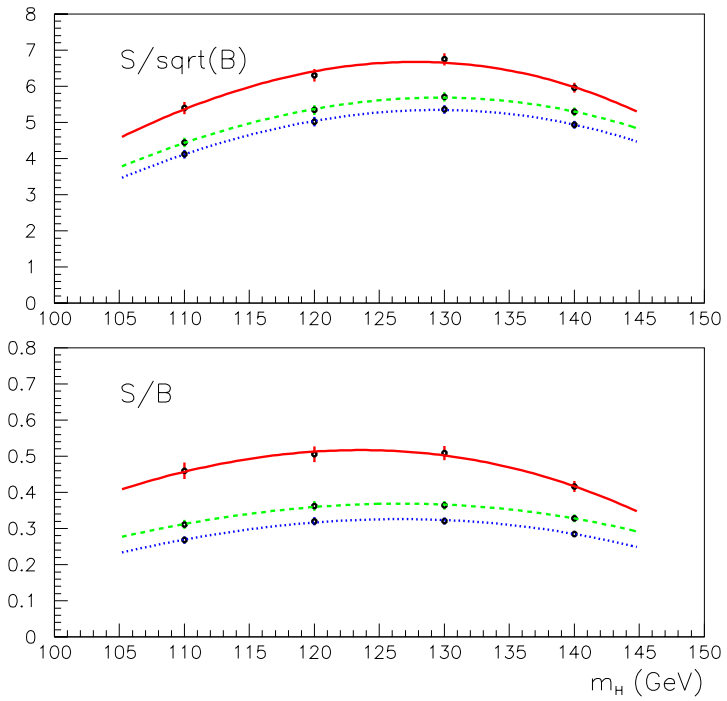

Fig. 8. The significance and the S/B ratio vs. m_H for an integrated luminosity of 30 fb^{-1} for $M_{\gamma\gamma jet} > 300$ GeV. The parton showering for background was generated with $Q^2 = (p_T^{q(g)})^2$ (solid line), $Q^2 = 0.5M_{\gamma\gamma}^2 + (p_T^{q(g)})^2$ (dashed line) and $Q^2 = M_{\gamma\gamma}^2 + 2(p_T^{q(g)})^2$ (dotted line).

References

[1] The ALEPH Collaboration, Phys. Lett. **B526**, 191 (2002).

[2] The DELPHI Collaboration, Phys. Lett. **B499**, 23 (2001).

[3] The OPAL Collaboration, Phys. Lett. **B499**, 38 (2001).

[4] The L3 Collaboration, Phys. Lett. **B517**, 319 (2001).

[5] The ATLAS collaboration, ATLAS Detector and Physics Performance TDR, CERN/LHCC/99-15 (1999).

[6] S. Abdullin, M. Dubinin, V. Ilyin, D. Kovalenko, V. Savrin and N. Stepanov, Phys. Lett. **B431**, 410 (1998).

[7] V. Zmushko, ATLAS Note ATL-PHYS-99-014 (1999).

[8] T. Sjostrand, Computer Physics Commun. **82** (1994) 74; S. Mrenna, preprint ANL-HEP-PR-96-63 (1996).

[9] T. Sjostrand, P. Eden, C. Friberg, L. Lonnblad, G. Miu, S. Mrenna and E. Norrbin, Computer Physics Commun. **135** (2001) 238; T. Sjostrand, L. Lonnblad and S. Mrenna, LU TP 01-21 [hep-ph/0108264].

[10] A. Pukhov et al., preprint INP-MSU-98-41-542 (1999).

[11] E. Richter-Was, D. Froidevaux and L. Poggioli, ATLAS Notes, ATL-PHYS-No-079 (1995), ATL-PHYS-No-131 (1998).

[12] G. Miu and T. Sjostrand, Phys. Lett. **B449**, 313 (1999).

[13] The D0 Collaboration, B. Abbott et al.,Phys. Rev. Lett. **80**, 5493 (1993).

[14] M. Spira, preprint CERN-TH/97-68 (1997).

[15] D. de Florian, M. Grazzini and Z. Kunszt, Phys. Rev. Lett. **82**,.5209 (1999).

[16] D. de Florian и Z. Kunszt, Phys. Lett. **B460**, 184 (1999).

[17] T. Plothow-Besch, Computer Physics Commun. **75** (1993) 396, Int. J. Mod. Phys. **A10** (1995) 2901.

Received June 13, 2002

Препринт отпечатан с оригинала-макета, подготовленного автором.

В.В. Змушко
Поиск $H \to \gamma\gamma$ в реакции $pp \to H + jet + X$ при $\sqrt{s} = 14$ ТэВ.

Оригинал-макет подготовлен с помощью системы LaTeX.

Подписано к печати 17.06.2002. Формат $60 \times 84/8$.
Офсетная печать. Печ.л. 1.62. Уч.-изд.л. 1.3. Тираж 160. Заказ 102.
Индекс 3649. ЛР №020498 17.04.97.

ГНЦ РФ Институт физики высоких энергий
142284, Протвино Московской обл.

Индекс 3649

П Р Е П Р И Н Т 2002–23, И Ф В Э, 2002